Impact of beam misalignment on THz wireless systems

Joonas Kokkoniemi[a,*], Alexandros-Apostolos A. Boulogeorgos[b], Mubarak Aminu[a], Janne Lehtomäki[a], Angeliki Alexiou[b], Markku Juntti[a]

[a]Centre for Wireless Communications (CWC), University of Oulu, P.O. Box 4500, 90014 Oulu, Finland
[b]Department of Digital Systems, University of Piraeus, Piraeus 18534, Greece

Abstract

This paper focuses on deriving expected values for the transmit (TX) and receive (RX) antenna gains in terahertz (THz) wireless fronthaul and backhaul links under stochastic beam misalignment, which is created by antenna movement coming from the building or antenna mast swaying. In particular, four different antenna movement models are considered: (i) Gaussian motion of a single antenna; (ii) Gaussian motion of both the TX and RX antennas; (iii) 2-dimensional (2D) Gaussian motion of a single antenna; and (iv) 2D Gaussian motion of the one antenna and one-dimensional Gaussian motion of the other. Models (i) and (iii) depict fronthaul scenarios, in which the access point is usually installed in high buildings or in road-sides. Models (ii) and (iv) may model backhaul applications. To verify the analysis and quantify the impact of beam misalignment, analytic and simulations results are provided that reveal that the antenna motion can cause a significant degradation on the expected value of the TX and RX antenna gains. Moreover, the derived models are used in a link budget assessment and insightful results for a number of realistic scenarios are given. These result clearly highlight the impact of beam misalignment in the received signal quality as well as the importance of taking into account the beam misalignment and using the correct antenna movement model, when evaluating its impact.

Keywords:
Antenna misalignment, THz backhauling, THz communications, THz fronhauling

1. Introduction

In order to counterbalance the spectrum scarcity problem, the beyond fifth generation wireless networks are expected to use pencil-beam high-frequency millimeter wave (mmW) and terahertz (THz) band links for fronthaul and backhaul applications [1, 2]. The THz band provides an extremely large amount of license-free spectrum, but the communication links in this band suffer from high channel attenuation. This forces utilization of extremely high-gain antennas and thus the employment of pencil-beamforming approaches[2]. However, the pencil-beamforming comes with challenges on beam acquisition, which, in realistic scenarios, is not perfect, causing significant link quality degradation [4]. As a consequence, beam misalignment is considered one of the main bottlenecks of THz wireless networks.

To bring a solution to the aforementioned problem, a great deal of research effort has been put on theoretically and experimentally analysing the impact of beam misalignment on mmW and THz wireless systems, as well as proposing beam tracking approaches [5–9]. The impact of deterministic beam misalignment on the ergodic capacity of a mmW ad-hoc network was studied in [5]. On the other hand, in [6], Priebe *et al.* evaluated the impact of beam misalignment through Monte Carlo simulations in terms of effective antenna gains and the effective resulting path losses. They assumed that the

---

*Corresponding author
Email addresses: joonas.kokkoniemi@oulu.fi (Joonas Kokkoniemi), al.boulogeorgos@ieee.org (Alexandros-Apostolos A. Boulogeorgos), mubarak.aminu@oulu.fi (Mubarak Aminu), janne.lehtomaki@ee.oulu.fi (Janne Lehtomäki), alexiou@unipi.gr (Angeliki Alexiou), markku.juntti@oulu.fi (Markku Juntti)

---

[2]To establish a 850 m link in the 240 GHz band, 50 dBi transmission (TX) and reception (RX) antenna gains are required [3].

misalignment angles in the azimuth and elevation with respect to the main beam direction can be modeled as uncorrelated Gaussian random processes. In [7], Lee *et al.* experimentally assessed the power losses due to beam steering misalignment. Their results verified that even a small beam misalignment causes a notable received power degradation. Additionally, in [8], wind effects on beam misalignment in mmW backhauling setups were investigated. They proposed a computationally efficient beam-alignment technique that samples the channel subspace adaptively by employing hierarchical codebooks. Finally, in [9], Boulogeorgos *et al.* investigated the impact of beam misalignment in THz wireless backhaul systems assuming that the RX antenna experiences 2-dimensional (2D) Gaussian motion while the TX is static. To sum up, most of the aforementioned contributions studied the impact of the beam misalignment in mmW and THz wireless backhauling systems, assuming different antenna motion models.

To the best of the authors' knowledge, a comparative study between the impact of beam misalignment, caused by different antenna motions has not been addressed in the technical literature. Aspired by this, in the present contribution we focus on extracting expected values for the TX and RX antenna gains in THz wireless fronthaul and backhaul links under stochastic beam misalignment assuming four different antenna motion models. Namely: (i) Gaussian motion of a single antenna; (ii) Gaussian motion of both the TX and RX antennas; (iii) 2-dimensional (2D) Gaussian motion of a single antenna; and (iv) 2D Gaussian motion of the one antenna and one-dimensional Gaussian motion of the other. Note that models (i) and (iii) accommodates fronthaul scenarios, in which the access point is usually installed in high buildings or in road-sides, while (ii) and (iv) may model backhaul applications. Our analysis is verified through respective Monte Carlo simulations that quantify the impact of beam misalignment and reveals that the antenna motion can cause significant degradation on the expected value of the TX and RX antenna gains. Moreover, we translate the derived antenna gains models into link-budget (LB) in order to evaluate the received signal quality. In this direction, we present insightful results that assess the LB in a number of realistic scenarios. Our results clearly highlight the impact of beam misalignment in the received signal quality as well as the importance of taking into account the beam misalignment and using the appropriate antenna motion model when assessing its impact.

In general, the problem of random motion to antennas becomes very important problem in the high frequency, high gain systems that depend on constantly available high antenna gains. This paper analyses the impact of the motion statistics on the performance. These affect communications of all scales. We mainly discuss backhaul and fronthaul communications. However, it will be shown that the movement statistics herein have greater impact on short distances than on longer distances.

The rest of this paper is organized as follows. Section 2 gives the path loss model of this paper, Sec. 3 goes into the antenna movement and misalignment models, and Sec. 4 derives the expected antenna gains from the stochastic antenna movement models. In Sec. 5, numerical results are provided accompanied by the respective discussion and insightful observations and finally, Sec. 6 summarizes and concludes the paper.

2. Path Loss Model

Due to focus on backhaul and fronthaul communications, we assume the common line-of-sight (LOS) path loss model to calculate the channel path gain, i.e., the channel coefficient $H(f, r, \theta)$. In the THz band, this is formed of the free space path loss (FSPL) according to the Friis transmission equation and the molecular absorption loss [10]

$$\mathrm{H}(f, r, \theta) = \frac{c^2}{(4\pi r f)^2} e^{-\kappa_a(f)r} G_{Tx}(\theta) G_{Rx}(\theta), \quad (1)$$

where c is the speed of light, r is the distance between Tx and Rx, f is the frequency, $\exp(-\kappa_a(f)r)$ is molecular absorption loss where $\kappa_a(f)$ is the frequency dependent molecular absorption loss coefficient, which can be estimated, e.g., as we have done in [11] or by utilizing the full line-by-line models [12], and $G_{Tx}(\theta)$ and $G_{Rx}(\theta)$ are the Tx and Rx gains, where θ is the observation angle. In the systems where the antennas are perfectly pointed at each other, the antenna gains are usually taken as the maximum gains. We focus on the case where the antennas are not stationary but moving. Then the expected antenna gain needs to be evaluated over the movement statistics. With uncertainty in the antenna gains and assuming that antenna gains at transmitter and receiver are uncorrelated (i.e., $\mathbb{E}[XY] = \mathbb{E}[X]\mathbb{E}[Y]$ where $\mathbb{E}[\cdot]$ is the expected value), the expected channel coefficient can be expressed as

$$\mathbb{E}[\mathrm{H}(f, r)] = \frac{c^2}{(4\pi r f)^2} e^{-\kappa_a(f)r} \mathbb{E}_\Phi[G_{Tx}(\Theta)] \mathbb{E}_\Phi[G_{Rx}(\Theta)], \quad (2)$$

where $\mathbb{E}_\Phi[G_{Tx}(\Theta)]$ and $\mathbb{E}_\Phi[G_{Rx}(\Theta)]$ are the expected Tx and Rx antenna gains, respectively, over certain antenna misalignment PDF Φ and with the random antenna directions Θ drawn from Φ. The antenna misalignment

PDFs are derived below along with how to obtain these expectations.

We utilize the common Johnson-Nyquist thermal noise term

$$P_n = \int_W k_B T df \approx k_B T W, \qquad (3)$$

where W is the bandwidth of the signal, k_B is the Boltzmann constant, and T is the temperature. Putting the channel model together, the signal-to-noise ratio (SNR) at the receiver becomes

$$\text{SNR}(f, r) = \frac{P_{\text{Tx}} \mathbb{E}[\text{H}(f, r)]}{P_n}, \qquad (4)$$

where P_{Tx} is the transmitted power.

3. Beam Misalignment Models

The antennas are usually assumed to be stationary and the problem is mostly in acquiring the correct direction to maximize the antenna gain and thereby also the link quality and performance. However, in practice, the antennas experience stochastic motion mainly due to environmental effects such as wind, small earthquakes, traffic etc., which are translated into beam misalignment. When the gain of the antenna gets higher, such as in the millimeter wave and THz systems, the narrow antenna beams become more vulnerable to random antenna movement. Motivated by this, we present stochastic antenna motion models in this section. We consider four different types of antenna movements: Gaussian, double-Gaussian, Rayleigh, and Gaussian-Rayleigh type movement. The Gaussian case corresponds to a scenario in which one antenna is stationary and the other experiences one dimensional (1D) swaying that can be modeled as a Gaussian process. In other words, we assume that in each time slot, the 1D pointing error can be modeled as a random variable (RV) that follows a Gaussian distribution[3]. To further elaborate this assumption (which is also true for the other motion statistics herein), the antenna movement is very low compared to the sampling frequency of the channel. Therefore, the antenna motion is highly correlated in time. However, in this paper, we calculate the expected antenna gains in the presence of antenna motion. The expected gain is taken as a long term average. This leads to expected gain appear as if there was no time

correlation. In reality, the antenna gain in the presence of the antenna motion would vary from very good to very low. The average expected gain, however, is obtained from the long time average.

The Gaussian motion corresponds to antenna swinging at one end of the link. The double-Gaussian case refers to a scenario where both the TX and the RX suffer from independent 1D Gaussian swaying. The Rayleigh case models 2D, i.e., up-down and left-right, independent swaying or shaking. This would correspond roughly to an earthquake or some other physical motion shaking the antenna. Finally, the last case corresponds to the scenario in which the other end is swaying according to Gaussian motion and the other one is shaking according to Rayleigh motion. The considered antenna movement cases are illustrated in Fig. 1. The corresponding models for the four motion types and combinations analysed in this paper are detailed below.

3.1. Gaussian Movement

The PDF of the Gaussian movement can be obtained as

$$f_g(x) = \frac{1}{\sqrt{2\pi\sigma_s^2}} e^{\frac{x^2}{2\sigma_s^2}}, \qquad (5)$$

where x stands for the antenna displacement, and σ_s^2 is the spatial jitter variance. Notice that we assume that the Gaussian movement is perfectly horizontal and the jitter variance describes the antenna swaying variance.

3.2. Double-Gaussian Movement

Both ends of the link swing in the double-Gaussian model. Due to the antenna motion independence, this case can be modelled similarly as in the case of single side movement, but by applying the Gaussian movement PDFs to the both antennas. Otherwise the PDFs are the same as in above Gaussian movement.

3.3. Two Dimensional Shaking

In this section, we examine an interesting scenario in which only the TX antenna experiences 2D shaking. We assume that the RX antenna has a circular effective area, A, of radius α. Similarly, the footprint of the TX circular beam at distance r equals ρ. Note that ρ belongs in the interval $0 \leq \rho \leq w_r$, where w_r represents the maximum radius of the beam at distance r. Furthermore, both the RX antenna effective areas and the TX beam footprint are considered on the positive $x - y$ plane of a Cartesian coordinate system and $\mathbf{z}$ is the pointing error, which can be expressed as the radial distance of the transmission and reception beams. Due to the symmetry of the beam

---

[3]This is a commonly accepted assumption that have been used in several previously published works (see, for example, [9, 13–19] and references therein.
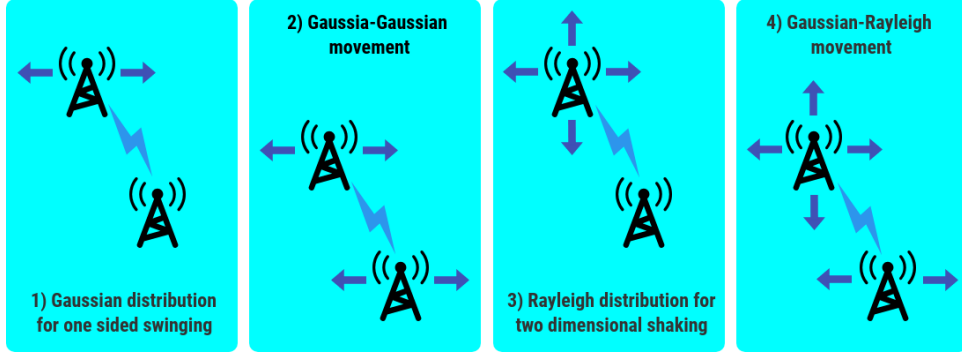
Figure 1: Illustration of the four considered cases antenna movement cases.

shapes, the beam misalignment coefficient, h_p, which returns the fraction of power that can be collected by the RX antenna, depends only on the radial distance, i.e., $z = |\mathbf{z}|$.

By considering independent and identical Gaussian distributions for the elevation and horizontal displacement [20–22], the radial displacement at the RX is proven to follow a Rayleigh distribution with PDF that can be obtained as

$$f_z(x) = \frac{x}{\sigma_s^2} \exp\left(\frac{x^2}{2\sigma_s^2}\right), \qquad (6)$$

where σ_s^2 is the variance of the pointing errors. Note that this model was extensively used in several studies in free space optical systems (see e.g., [23, 24] and references therein) as well as in THz wireless systems [22].

Based on [20], h_p can be approximated as

$$h_p(x; r) \approx A_o \exp\left(-\frac{2x^2}{w_{eq}^2}\right), \qquad (7)$$

where w_{eq} stands for the equivalent beamwidth, r is the transmission distance, and A_o is the fraction of the collected power at $x = 0$, which can be calculated as

$$A_o = (\mathrm{erf}\,(v))^2, \qquad (8)$$

with

$$v = \frac{\sqrt{\pi}a}{\sqrt{2}w_r}. \qquad (9)$$

In (9), a is the radius of the RX effective area and w_r is the radius of the TX beam footprint at distance r. Moreover, w_{eq}^2 is related to the squared beamwidth at distance r, w_r^2, through

$$w_{eq}^2 = w_r^2 \frac{\sqrt{\pi}\mathrm{erf}\,(v)}{2v \exp\,(-v^2)}, \qquad (10)$$

where $\mathrm{erf}\,(\cdot)$ stand for the error function.

3.4. Gaussian-Rayleigh Movement

In the Gaussian-Rayleigh case, the one end of the link is swinging according to the Gaussian motion and the other end is shaking according to the Rayleigh motion. As in the double Gaussian, due to independence of the antennas, the motion statistics are applied to the both ends independently. We could also in the same way study a double Rayleigh scenario, where both transmission ends would experience 2D motion. This can be obtained by utilizing the Rayleigh distribtion independently to the Rx and Tx antenna gains. However, this scenario is seen as the most rare among the cases here and is not analyzed in this paper. It could be possible in the case of two handheld devices, but with limited motion variance. This cases is left for the specific case study for some research group that might consider a scenario where this motion would be relevant.

3.5. The Parameters for the Simulations

The two fundamental motion mechanisms considered in this paper, namely, the PDFs of the Gaussian and Rayleigh motions are illustrated in Fig. 2. The x-axis in Fig. 2 shows the physical displacement of the antenna from the zero-position due to movement with few motion variances. In this paper, we utilize jitter variances from 0.01 to 0.2 m^2. Those correspond to extreme displacement from about 25 cm to about 1.5 m. The chosen range for the jitter variance is mostly based on illustrating antenna movement from low to extreme. These values, however, fit quite well to movement of the real structures, such as high buildings, high antenna masts, an antenna on top of a cruise ship on stormy ocean, or even a user holding a device. There are large numbers of possible application where the models presented herein can be utilized. The focus herein is on the stochastic modelling of the antenna movement rather than any specific scenario. However, the chosen range of jitter vari-
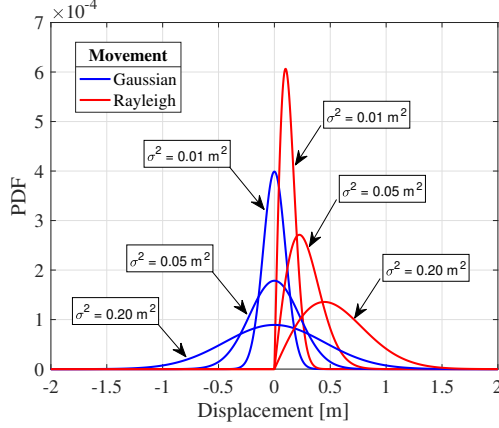
4

Figure 2: PDFs of the Gaussian and Rayleigh misalignment for jitter variances of 0.05, 0.1 and 0.2 m^2.

Figure 3: Antenna array factors of the ULA model utilized in this paper for 32, 256, and 1024 element antenna arrays.

ances cover the most of the applications where the antenna movement may be an issue. The maximum variance of 0.2 m^2 with a maximum swing range of roughly ±1.5 meters is quite extreme and the most of the real world applications will experience lower movement.

4. Stochastic Antenna Gain

4.1. The Antenna Model

We assume uniform linear array (ULA) antennas at both the TX and RX whereby the antenna elements are placed linearly and separated by equal distance d. The ULA assumption offers an easy way to compare the impact of antenna movement to the expected antenna gain. Mathematically, the antenna gain at a certain azimuth angle of observation α is given as

$$G(\alpha) = |AF(\alpha)|^2, \tag{11}$$

where $AF(\alpha)$ is the array factor. The array factor provides the far-field radiation pattern of ULA given as

$$
\begin{aligned}
AF(\alpha) &= \boldsymbol{\beta}(\Gamma)^H \mathbf{a}(\alpha) \\
&= \frac{1}{\sqrt{N}} \sum_{n=0}^{N-1} e^{j\frac{2\pi}{\lambda} dn(\sin(\alpha) - \sin(\Gamma))},
\end{aligned}
\tag{12}
$$

where $\mathbf{a}(\alpha)$ is the steering vector, and λ and d (= $\lambda/2$), where λ is the wavelength, are the carrier wavelength and spacing between the antenna elements, respectively. $\boldsymbol{\beta}(\Gamma)$ is a vector consisting of the beamforming weights (constant amplitude for the phased array herein) and Γ is the desired beam steering direction. Example responses of such array ($\Gamma = 0$) for 32, 256, and 1024 antenna elements are given in Fig. 3. These patterns are also
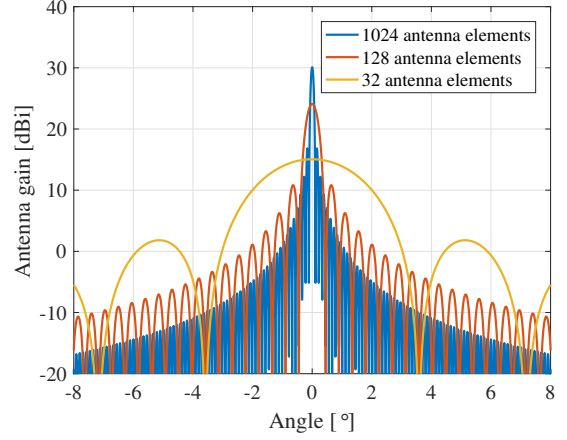
considered in the numerical results as they give good range of different antenna gains and beamwidths. In real life, with $\lambda/2$ antenna spacing, these antenna arrays would have sizes ranging from 1.6 cm to 51.2 cm for 32 to 1024 element arrays, respectively, at 300 GHz carrier frequency. The linear phased array antenna's maximum achievable gain is equivalent to the number of antenna elements due to constructive summation of the individual antenna element gains at the beamforming direction (given the antenna element phases are perfectly adjusted). In the ideal case, the antenna patterns of each antenna element can be considered on the average equal, and thus, the maximum gain is a sum over the antenna elements. This assumption is very accurate if the number of antenna elements is large [25]. Furthermore, the ULA antenna elements are assumed to be placed horizontally with each antenna element being a vertical dipole element giving omnidirectional pattern in azimuth angle. The elevation radiation pattern of such ULA antenna is very wide. Therefore, the motion statistics described above are in valid for the motion seen on the azimuth angle from the broadside of the antenna.

4.2. Stochastic Antenna Misalignment

As mentioned above, the antenna movement causes the antenna pattern to deviate from the maximum gain given the antennas at the Tx and Rx are perfectly pointed toward each other. The expected antenna gain is calculated as an expectation over the antenna pattern and the movement statistics. The movement statistics were discussed in the previous section as well as the assumptions on those. From the expected antenna gain

point of view, the statistics could be provided by any PDF describing the antenna gain pattern and the movement of the antenna(s). The expected antenna gain is obtained as

$$\mathbb{E}_\Phi[G(\Theta)] = \int_\theta \Phi(\theta)G(\theta)d\theta, \qquad (13)$$

i.e., as an integral over the antenna pattern and the PDF $\Phi(\theta)$ of the antenna movement.

The PDFs for the movement scenarios herein are $\Phi_g(\theta) = f_g(\theta)$ and $\Phi_r(\theta) = f_r(\theta)$ for the Gaussian and Rayleigh distributions, respectively. Due to the independence of the Rx and Tx antennas, the combinations of the antenna statistics are calculated separately for the both ends, Tx and Rx. The distributions $f(x)$ in this paper are for the radial displacement of the antenna gain due to the motion. We need to map those to the antenna directions by calculating the transformation $x \to \theta$. This map can be done simply by trigonometry

$$\theta = \arctan\left(\frac{x}{r}\right), \qquad (14)$$

where r is the distance between Tx and Rx, and x is the displacement. Figure 2 above shows the displacement for the considered Gaussian and Rayleigh distributions with 0.01, 0.05 and 0.2 m² jitter variances. The above equation also gives away the fact that the antenna's angular displacement will be less severe for the same radial displacement as the distance is increased. This is intuitively expected as the same, e.g., lateral movement looks the larger the closer-by the observer is to the moving object. If, however, one would consider pivotal movement, the situation would change. The further away subject would experience a larger deviation in the antenna gain. Otherwise, the basic modelling would be the same: the expected antenna would be an integral over the pivotal angle and the movement statistic. However, in this paper and in the numerical results we focus on the radial displacement type of a movement.

One could visualize the impact of the movement PDF versus the expected antenna gain with the given antenna patterns in Fig. 3. Assume that the 1024 element ULA gives the antenna pattern and the 32 element ULA depicts the PDF of the antenna motion. It is obvious that the maximum gain of the antenna would drop sharply due to averaging over such large angular range. Turning the situation other way around, i.e., the 1024 element ULA depicting the PDF of the movement and the 32 element ULA the antenna gain, the impact of the motion would be very small. The minor deviation from the maximum gain still keeps the average gain at feasible level. This is also shown in the numerical results where

the 32 antenna array with low gain suffers considerably less of the motion than the 1024 element array. This is an expected result, but shows some interesting SNR and capacity behavior between the different antenna gains.

5. Numerical Results

The impact of the antenna misalignment to the expected antenna gain and performance of the point-to-point link is analysed in this section. The simulation parameters used to calculate the numerical results are listed in Table 1. The center frequency of the transmission was 300 GHz with 10 GHz bandwidth. The transmit power was 0 dB. The noise power was calculated for 296 K noise temperature. The antenna configurations were 32, 256, and 1024 antenna element ULAs that correspond to single side antenna gains of about 15, 24, and 30 dBi, respectively. The half power beamwidth (HPBW) of a phased array can be estimated in radians by [26]

$$\alpha_{3\text{dB}} = 0.886\frac{\lambda}{N_{Tx}d} = \frac{1.772}{N_{Tx}}, \qquad (15)$$

where $\alpha_{3\text{dB}}$ is the HPBW and the last term is for the utilized antenna element spacing of $d = \lambda/2$ and N_{Tx} is the number of the antenna elements in ULA. This approximation was verified to be accurate for the phased array described above and for the antenna configurations described on Table 1. Notice that the approximation of the HPBW is dependent on the antenna type and the above one is valid for linear phased arrays. In the simulations, each of the motion statistics were calculated assuming the same antenna configuration in both ends (Rx and Tx).

Figures 4 to 6 show the expected antenna gains for 32, 256, and 1024 element antenna arrays, respectively, for the four movement cases presented above and as a function of the movement variance. The illustrated losses are for the combined Rx and Tx gains. The gains of the antenna arrays were kept equal at both sides. The severity of the movement to the total antenna gain strongly depends on the antenna gain, i.e., how narrow is the main lobe beam and on the distance between Tx and Rx. The narrower is the beam, the more the movement has impact on the gain. As the distance increases, the relative motion becomes smaller and the impact of the movement to the antenna gain is also smaller. This is because of relative motion of an object to an observer seems smaller as the distance increases. On the other hand, from the antenna gain point of view, over longer distances the energy spreads more and the Tx illuminates larger area.

The antenna gain plays an important role in the gain degradation. We use antenna arrays in the analysis herein. The antenna arrays are strongly focused towards the steered direction. We can see in Figs. 5 and 6 that the relative gain loss is much higher in the case of 1024 element array compared to that of the 256 element array. Over a 100 meter link, the 1024-element array gives on par or lower gain than 256 element array. This is because the 3-dB beamwidth of the larger array is four times smaller (0.1 vs. 0.4 degrees). We can see in Fig. 7 how even very small movement causes a severe impact on the total antenna gain of the 1024 element array and especially compared to 256 element array. Especially the most severe movement, the Gaussian-Rayleigh is very sensitive to the movement with the gain dropping very fast for high number of antenna elements.

For the 32 element array, the impact of the movement over long distances is negligible. This follows the much higher 3-dB beamwidth of 3.2 degrees. In this case, similarly as for the higher antenna element cases, the movement causes larger loss for the shorter distances. Comparing the worst case scenarios, namely the Gaussian-Rayleigh cases for 20 meters at 0.2 m^2 motion variance, the total antenna gain losses for the link budget are 4, 25, and 40 dBs for the 32, 256, and 1024 element arrays.

In general, it can be concluded that the 3-dB beamwidth plays an important role in how severe loss the the antenna movement causes. Very high gain antennas therefore suffer more from the movement as it could be expected. It should be remembered that the 3-dB beamwidth does not only depend on the antenna gain, but also on the antenna structure and the shape of the beam. Thus, the possible impact of the movement
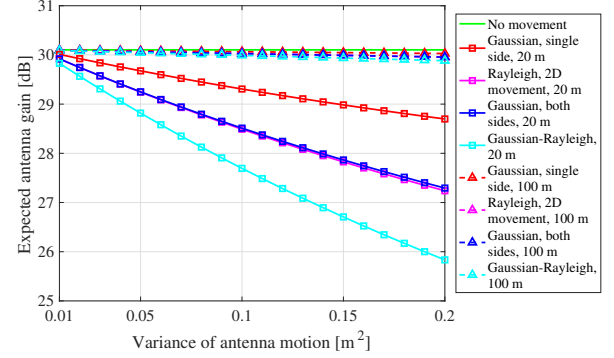

Figure 4: The expected antenna gain with and without antenna movement for 32-antenna array.
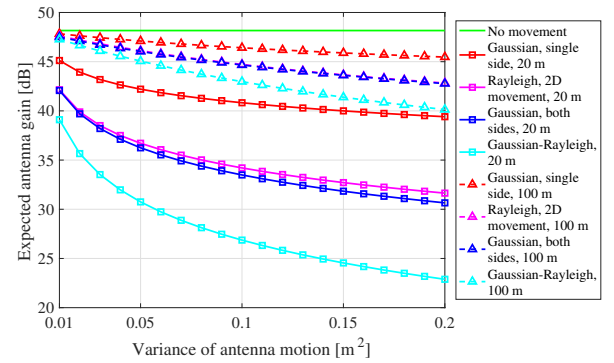

Figure 5: The expected antenna gain with and without antenna movement for 256-antenna array.
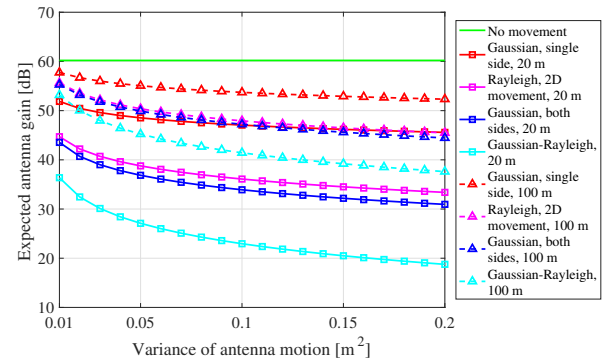

Figure 6: The expected antenna gain with and without antenna movement for 1024-antenna array.

to the link budget need to be considered for each application and the type of antennas that are utilized therein.

Figures. 8 to 10 show the above total antenna gains' impact on the SNR as a function of distance for the movement variance of 0.05 m^2 and 0.2 m^2. As expected
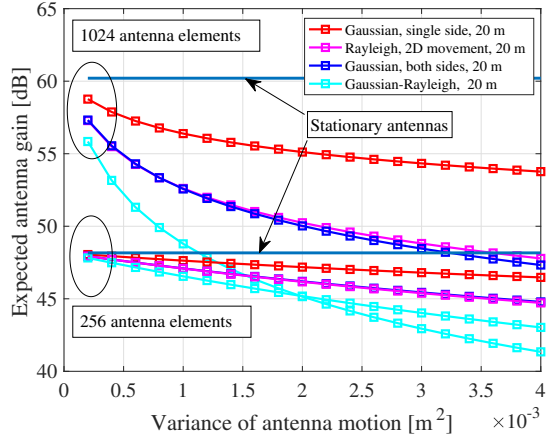
Figure 7: Comparison of the expected antenna gains for very small antenna movement between 256-antenna array and the 1024-antenna array.
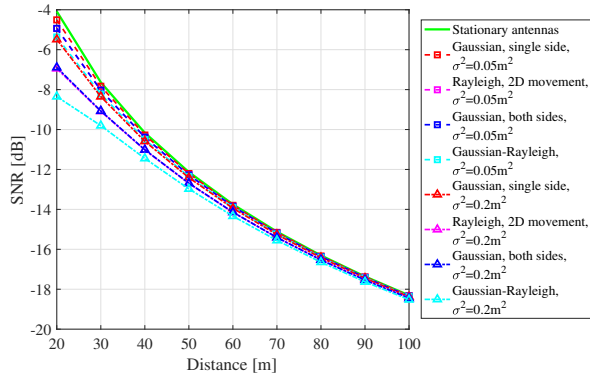

Figure 8: The expected SNR with and without antenna movement for 32 element antenna array.
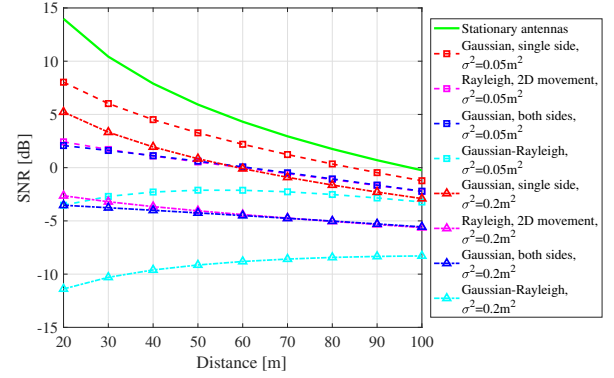

Figure 9: The expected SNR with and without antenna movement for 256 element antenna array.
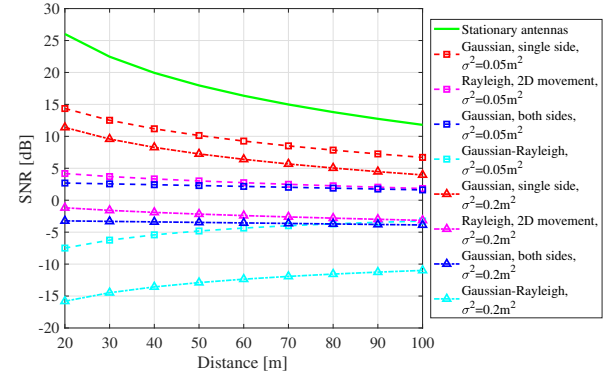
Figure 10: The expected SNR with and without antenna movement for 1024 element antenna array.

from above, the antenna gain has a major impact on the SNR and how it behaves. As it was shown above, the severity of the movement and the 3-dB beamwidth have major impact on the expected gain of the system. The expected antenna gain tends to be higher at larger distances and this is also visible in Figs. 8 to 10. The longer distance in general suffer relatively lower gain loss in the presence of movement. This in the extreme cases leads to SNR increasing as a function distance as the antenna gain increases faster than the path loss. However, this is only true for the extreme movement cases with very large antenna arrays, such as Gaussian-Rayleigh movement with 256 and 1024 element antenna arrays.

The antenna gains considered here are rather low for long distance links at 300 GHz. This shows as negative and low SNRs at long distance links. Especially the

32 element array provided gains that would be adequate mostly for very short distance link, such as in-room communications. However, these figures also show the vulnerability of the THz frequency link budgets to any unwanted additional losses. The designed system may operate well in ideal conditions, but adding, for instance, a storm that shakes the antenna may render the link unusable. the results herein do not take into account the coding that would be able to correct burst errors. On the other hand, high bandwidth systems sample the channel very fast compared to a physical movement. Therefore, the error bursts can be expected to be very long compared to channel codes' ability to fix the errors. The correlation of the movement and the channel sampling is not considered here. The results herein depict long term average expected values. Thus, the negative SNR does not mean that the channel is constantly unusable, it is just unusable for the most of the time. The antenna movement therefore sets application specific re-

Table 2: Link budget values for the 1024 element antenna array for antenna movement variance of 0.05 m^2

Parameter	20 m link	100 m link
Transmit power	0 dBm	0 dBm
FSPL	108.1 dB	122.3 dB
Absorption loss	0.06 dB	0.3 dB
Noise power	-73.9 dBm	-73.9 dBm
Expected total antenna gain		
Stationary antennas	60.2 dBi	60.2 dBi
SNR	26.0 dB	11.8 dB
Gaussian	48.5 dB	55.1 dB
SNR	14.5 dB	6.7 dB
Rayleigh	38.4 dBi	50.2 dBi
SNR	4.2 dB	1.8 dB
Gaussian-Rayleigh	26.7 dBi	45.1 dBi
SNR	-7.5 dB	-3.3 dB

quirements on movement tracking, tracking speed, overall antenna gain, and the channel coding. These then ultimately set the boundaries for the highest modulation orders that can be utilized and therefore the achievable throughput.

Table 2 presents the link budget calculations for the 1024 element antenna array and with the movement variance of 0.05 m^2. This table gives a better insight on the impact of the antenna movement to the link budget. It can be seen that even with relatively low movement, the SNR decreases quite a bit when movement is introduced. From the link budget point of view, the antenna gain of about 30 dBi per side would be very tight for such link distances, but it also shows that if there is not much room to move in the link budget, external forces can take the system below operational link quality. A minor note here is that by choosing the center frequencies correctly, for instance here at 300 GHz, we can neglect the impact of the molecular absorption loss, which is at most 0.3 dB at 100 meter link distance.

Finally, Fig. 11 shows the calculated capacities for the 1024 element antenna array as a function of the distance and the antenna movement variance. We show the results for this particular antenna configuration since it best depicts the peculiar SNR behavior in the presence of antenna motion as shown above. The capacity is calculated as the familiar Shannon capacity

$$C = W \log_2(1 + \text{SNR}), \tag{16}$$

where C is the capacity and W is the bandwidth. We can see that the overall capacity is mostly following the expected trend with decreasing capacity with distance and movement variance. And exception is made by the Gaussian-Rayleigh movement that causes so large gain loss at short distances that the capacity actually increases as a function of distance. This is somewhat expected based on the above SNR values since the Shannon capacity mirrors the SNR performance. This is of course the extreme case that would require very large movement and equally interesting results are given by Rayleigh and Gaussian-Gaussian cases. These two movement cases flatten the SNR such that the capacity difference at lowest movement variance here at 0.01 m^2 was dropping from 35 Gbps to 26 Gbps when moving from 20 meter to 100 meter link distance for the Rayleigh movement and from 33 to 26 Gbps for the Gaussian-Gaussian movement. This is very low drop compared to for instant single side Gaussian movement where for the same movement variance leads to capacity drop from about 59 Gbps to 33 Gbps when moving from 20 meters to 100 meters. This is very interesting behavior, which is attributed partially to the extremely highly directional antennas used in the paper. However, the future mmWave and THz systems will require very high antenna gains for optimal operation, which forces to take into account the antenna movement in the link budget analysis as well as in the design if the tracking algorithms.

6. Conclusion

We studied the stochastic behavior of the antenna misalignment. Three different movement models were utilized in the analysis. It was shown that the distance between the antennas is one important factor herein, since the relative moment of the antenna depends on the distance. The same movement is relatively more severe at short distances than in the longer ones due to the angular dispersion of the radial displacement of the antenna is less significant. The results in this paper showed that the antenna movement may degrade the expected antenna gain significantly. This makes the backor fronthaul link more vulnerable to increased bit errors, causes need for higher coding and lower modulation orders, and causes lower overall capacity. The antenna gain plays an important role herein as very the wide beamwidths of low gain antennas do not experience the antenna displacement as strongly as very narrow beamwidths of highly directional antennas. The random motion on high frequency, high gain systems may require new tracking algorithms in order to minimize the link performance hit in those scenarios and cases when external forces causes additional movement. This type of random motion can be caused by many source such as in the case where a car is driving on
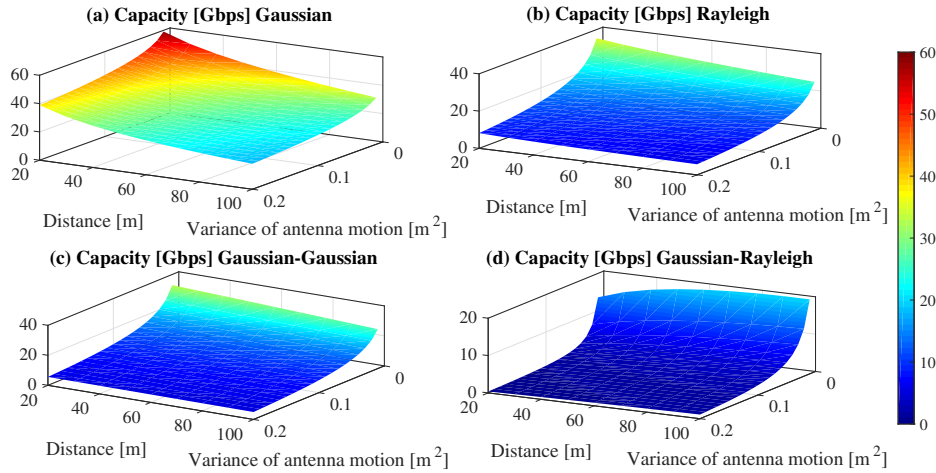
Figure 11: The expected capacity of the link as a function of distance and antenna movement variance for 1024 element antenna array.

rough surface (general movement plus shaking), during windy weather (antenna swaying), or during an earthquake (shaking). Also, the antenna motion tracking during the random motion is an important problem as it is also the case when, for instance, person holds a phone. The device's orientation is constantly and randomly changing.

The results in this paper would be useful in studying various cases, such as in the backhaul link performance and link budget estimation, stochastic geometry models, and in other models where movement of the antennas is present. In the future work, we will extend the models to cover more severe movement in the cases where the antenna is held, e.g., by a user. Also, based on the models herein, it is easy to extend those to include any type of arbitrary movement and various realistic antenna patterns for different applications.

References

[1] T. S. Rappaport, et al., Millimeter wave mobile communications for 5G cellular: It will work!, IEEE Access 1 (1) (2013) 335–349.

[2] I. F. Akyildiz, J. M. Jornet, C. Han, Terahertz band: Next frontier for wireless communications, Elsevier Phys. Commun. 12 (2014) 16–32.

[3] I. Kallfass, F. Boes, T. Messinger, J. Antes, A. Inam, U. Lewark, A. Tessmann, R. Henneberger, 64 Gbit/s transmission over 850 m fixed wireless link at 240 GHz carrier frequency, J. Infrared Milli. Terahz. Waves 36 (2) (2015) 211–233.

[4] J. Zhang, X. Ge, Q. Li, M. Guizani, Y. Zhang, 5g millimeter-wave antenna array: Design and challenges, IEEE Wireless Communications 24 (2) (2017) 106–112. doi:10.1109/MWC.2016.1400374RP.

[5] A. Thornburg, R. W. Heath, Ergodic capacity in mmwave ad hoc network with imperfect beam alignment, in: MILCOM 2015 - 2015 IEEE Military Communications Conference, 2015, pp. 1479–1484. doi:10.1109/MILCOM.2015.7357653.

[6] S. Priebe, M. Jacob, T. Kürner, Affection of thz indoor communication links by antenna misalignment, in: 6th European Conference on Antennas and Propagation (EUCAP), 2012, pp. 483–487. doi:10.1109/EuCAP.2012.6206026.

[7] J. Lee, M.-D. Kim, J.-J. Park, Y. J. Chong, Field-measurement-based received power analysis for directional beamforming millimeter-wave systems: Effects of beamwidth and beam misalignment, ETRI Journal 40 (1) (2018) 26–38. doi:10.4218/etrij.2017-0188.

[8] S. Hur, T. Kim, D. J. Love, J. V. Krogmeier, T. A. Thomas, A. Ghosh, Millimeter wave beamforming for wireless backhaul and access in small cell networks, IEEE Trans. on Comm. 61 (10) (2013) 4391–4403. doi:10.1109/TCOMM.2013.090513.120848.

[9] A. A. Boulogeorgos, E. N. Papasotiriou, A. Alexiou, Analytical performance assessment of thz wireless systems, IEEE Access 7 (2019) 11436–11453. doi:10.1109/ACCESS.2019.2892198.

[10] J. M. Jornet, I. F. Akyildiz, Channel modeling and capacity analysis for electromagnetic nanonetworks in the terahertz band, IEEE Trans. Wireless Commun. 10 (10) (2011) 3211–3221.

[11] J. Kokkoniemi, J. Lehtomäki, M. Juntti, Simplified molecular absorption loss model for 275 – 400 gigahertz frequency band, in: Proc. European Conf. Antennas Propag., 2018, pp. 1–5.

[12] L. S. Rothman, et al., The HITRAN 2012 molecular spectroscopic database, J. Quant. Spectrosc. Radiat. Transfer 130 (1) (2013) 4–50.

[13] A.-A. A. Boulogeorgos, A. Alexiou, Error analysis of mixed THz-RF wireless systems, IEEE Communications Letters 24 (2) (2020) 277–281. doi:10.1109/LCOMM.2019.2959337.

[14] A.-A. A. Boulogeorgos, E. N. Papasotiriou, A. Alexiou, Analytical performance evaluation of thz wireless fiber extenders, in: IEEE 30th Annual International Symposium on Personal, Indoor and Mobile Radio Communications (PIMRC), 2019, pp. 1–6. doi:10.1109/PIMRC.2019.8904434.

[15] H. G. Sandalidis, T. A. Tsiftsis, G. K. Karagiannidis, M. Uysal, Ber performance of fso links over strong atmospheric turbulence channels with pointing errors, IEEE Communications Letters 12 (1) (2008) 44–46. doi:10.1109/LCOMM.2008.071408.

[16] H. G. Sandalidis, Coded free-space optical links over strong turbulence and misalignment fading channels, IEEE

Transactions on Communications 59 (3) (2011) 669–674. doi:10.1109/TCOMM.2011.121410.090318.

[17] M. P. Ninos, H. E. Nistazakis, H. G. Sandalidis, G. S. Tombras, Cdma rofso links with nonzero boresight pointing errors over m turbulence channels, IEEE Photonics Journal 10 (5) (2018) 1–12. doi:10.1109/JPHOT.2018.2856369.

[18] J. Park, E. Lee, C. Chae, G. Yoon, Impact of pointing errors on the performance of coherent free-space optical systems, IEEE Photonics Technology Letters 28 (2) (2016) 181–184. doi:10.1109/LPT.2015.2489383.

[19] E. Zedini, M. Alouini, Multihop relaying over im/dd fso systems with pointing errors, Journal of Lightwave Technology 33 (23) (2015) 5007–5015. doi:10.1109/JLT.2015.2492244.

[20] A. A. Farid, S. Hranilovic, Outage capacity optimization for free-space optical links with pointing errors, Journal of Lightwave Technology 25 (7) (2007) 1702–1710. doi:10.1109/JLT.2007.899174.

[21] S. Arnon, Effects of atmospheric turbulence and building sway on optical wireless-communication systems, Opt. Lett. 28 (2) (2003) 129–131. doi:10.1364/OL.28.000129.

[22] A.-A. A. Boulogeorgos, E. N. Papasotiriou, A. Alexiou, Analytical performance assessment of THz wireless systems, IEEE Access 7 (1) (2019) 1–18. doi:10.1109/ACCESS.2019.2892198.

[23] H. G. Sandalidis, T. A. Tsiftsis, G. K. Karagiannidis, Optical wireless communications with heterodyne detection over turbulence channels with pointing errors, Journal of Lightwave Technology 27 (20) (2009) 4440–4445.

[24] L. Yang, X. Gao, M.-S. Alouini, Performance analysis of relay-assisted all-optical FSO networks over strong atmospheric turbulence channels with pointing errors, J. Lightwave Technol. 32 (23) (2014) 4011–4018.

[25] Rohde & Schwarz, Millimeter-wave beamforming: Antenna array design choices & characterization (white paper), Tech. rep., Rohde & Schwarz (Oct. 2016).
URL http://www.rohde-schwarz.com/appnote/1MA276

[26] S. J. Orfanidis, Electromagnetic Waves and Antennas, Rutgers University, 2016.
URL www.ece.rutgers.edu/ orfanidi/ewa